Fibers and Polymers 2021, Vol.22, No.6, 1580-1593
DOI 10.1007/s12221-021-0543-7

ISSN 1229-9197 (print version)
ISSN 1875-0052 (electronic version)

Polyethyleneimine Modified Magnetic Microcrystalline Cellulose for Effective Removal of Congo Red: Adsorption Properties and Mechanisms

Jian Zhang, Changpo Ma, Hui Li, Ximo Wang, Feng Ning, Minxia Kang, and Zumin Qiu*

Key Laboratory of Poyang Lake Environment and Resource Utilization, Ministry of Education, School of Resources Environmental and Chemical Engineering, Nanchang University, Nanchang 330031, China

(Received May 12, 2020; Revised August 8, 2020; Accepted September 13, 2020)

Abstract: In this study, microcrystalline cellulose modified with Fe_3O_4 and polyethyleneimine (Fe_3O_4/MCC-PEI(70K-5)) was synthesized for Congo red (CR) adsorption. Various batch experiments were conducted to explore the effects of initial concentration, contact time, solution pH, and cationic concentration. The results showed that the adsorption process of CR onto Fe_3O_4/MCC-PEI(70K-5) were spontaneous and endothermic, and strictly followed pseudo-second-order and Freundlich models. The equilibrium time of CR adsorption onto Fe_3O_4/MCC-PEI(70K-5) at 298 K was 100 min and the maximum adsorption capacity was 862.25 mg/g. Zeta-potential, XPS, and FT-IR analyses proved that the adsorption behavior was primarily ascribed to the electrostatic interactions between Fe_3O_4/MCC-PEI(70K-5) and CR molecules. Additionally, Fe_3O_4/MCC-PEI(70K-5) has a good performance of regeneration and reuse, which maintained a high adsorption capacity even after five consecutive regenerations.

Keywords: Microcrystalline cellulose, Magnetic, Polyethyleneimine, Congo red, Adsorption mechanisms

Introduction

Dyes are the most common pollutants in wastewater because of its strong toxicity, non-biodegradability, and accumulation in plants, animals, and humans [1]. With the increasing diversity of industrial products, the composition of dye wastewater becomes more and more complex and its treatment has become an extremely difficult task. Congo red (CR), as one of the water-soluble anionic dyes, has been widely used in textile, leather, printing, cosmetics industries, and biomedical researches [2]. It can weaken the penetration of light in water and inhibit the photosynthesis ability of aquatic organisms, even at low concentrations, which can seriously affect aquatic organisms and food webs. In addition, it can also cause some health problems to humans and animals, such as difficulties in breathing, diarrhoea, vomiting, and nausea [3]. Therefore, effective removal of CR from wastewater is important to ensure human health.

Various methods including photocatalytic decomposition, membrane separation, adsorption, flocculation, electrolysis, and biological treatment have been studied to remove CR from wastewater [4-7]. Among these methods, adsorption is considered to be the best one, which is attributed to its simplicity of design, ease of operation, and higher efficiency. Therefore, the adsorption method has received much attention. Various adsorbents have been reported in the literature, such as multi-walled carbon [8], clay minerals [9], zeolites [10], metal-organic frameworks [11], and biomass [12]. However, separation from solution is not easy for most conventional adsorbents. To overcome this limitation, magnetic nanomaterials are widely used, which can be separated from the aqueous solutions by an external magnets. Fe_3O_4 nanoparticles are a common magnetic nanomaterial and are widely used in the preparation of adsorbents due to their small radius, superparamagnetism, and large surface area [13]. The Fe_3O_4 nanoparticles not only exhibit the outstanding magnetic property which can greatly simplify their collection from the complex multiphase systems under external magnetic fields, but also due to the anchoring of specific binding sites on the surface, the hybrid multifunctional nano-adsorbent loaded with Fe_3O_4 can improve the adsorption capacity [14,15]. In addition, efficiency is improved due to the common contact interface and synergy between the nanoparticles and the support.

However, nanoparticles tend to aggregate, which greatly reduces their efficiency in practical applications [16]. Inorganic and organic materials are commonly used to modify nanoparticles by physical coating, bonding, and chemical coating, and then improve the performance of magnetic nanomaterials [17]. Cellulose is the most widely used renewable biopolymer in nature and is a very promising low-cost raw material for the preparation of a wide range of functional materials. Microcrystalline cellulose (MCC) is one of the most important types of cellulose derivative, and because of its non-toxicity, large surface area, and biodegradability, it has become an attractive adsorbent for removing pollutants from wastewater. In addition, due to the chemical structure of cellulose, MCC has a lot of hydroxyl groups on its surface, resulting in high activity and ability to react with various specific groups [18]. Such properties gave MCC the flexibility in a variety of applications, including the removal of dyes from wastewater as an adsorbent.

Polyethylenimine (PEI) is a widely used cationic polymer which contains a large amount of amino groups in its main chain and branches. In addition, PEI molecules have excellent water solubility and are harmless to the environment.

*Corresponding author: mzqiu@ncu.edu.cn

Commercially available PEI usually contains primary, secondary, and tertiary amino groups in a ratio of 1:2:1 in the branches [19]. Furthermore, PEI is also a cationic polyelectrolyte due to its high charge density and good biocompatibility [20]. Hence, PEI has been widely used as a water treatment modifier to remove negatively charged contaminants from wastewater. In recent researches, the use of PEI for surface modification has become a popular method for improving the adsorption performance of adsorbent. You *et al.* [2] synthesized the PEI modified Fe_3O_4/CS as a desired adsorbent via crosslinking reaction for effective removal of Congo red from aqueous solution, while the crosslinking agent is not environment-friendly. Chemical crosslinking is one of the commonly used methods in the preparation of adsorbents. Epichlorohydrin and glutaraldehyde are often used as crosslinking agent, which is toxic and carcinogenic to creatures [21]. Wong *et al.* [22] obtained the PEI modified spent tea leaves as an adsorbent with impregnation method, and it has a good adsorption capacity except that the separation performance is not very satisfactory.

Accordingly, in order to overcome the disadvantage of separation and improve the adsorption capacity, Fe_3O_4 nanoparticles were synthesized to bond to MCC with one-pot method. Then, PEI as a modifier further increased the adsorption capacities. The fabricated Fe_3O_4/MCC-PEI(70K-5) was characterized by a variety of methods, such as SEM, TEM, EA, XRD, FT-IR, BET, VSM, and TG. The adsorption process of CR onto Fe_3O_4/MCC-PEI(70K-5) was studied. Based on the adsorption kinetics, isotherms, and thermodynamics, the possible adsorption mechanism was proposed.

Experimental

Materials

Congo red was purchased from Solarbio Biotechnology Co., Ltd. Microcrystalline cellulose (≤ 65 μm) was provided by Qingdao Yousuo Chemical Technology Co., Ltd. Polyethyleneimine (Molecular weight=1.8K, 10K, 70K) was provided by Shanghai Macklin Biochemical Technology Co., Ltd. All other chemicals were of analytical reagent grade and deionized water produced by an ultrapure water system (Millipore, Bedford, MA, USA) was used to prepare all solutions.

Adsorbent Preparation and Characterization

Preparation of Fe_3O_4/MCC

Fe_3O_4/MCC was obtained by a one-pot method [21]. In detail, 0.900 g MCC was added into 60 m*l* ethanediol and ultrasonicated (120 W) for 30 min to form suspension A and 3.000 g $FeCl_3 \cdot 6H_2O$ and 6.000 g NaOAc were poured into 60 m*l* ethanediol and ultrasonicated for 30 min to obtain mixture B. After that, suspension A and mixture B were ultrasonically mixed for another 30 min, then the final mixture was transferred into a Teflon-lined stainless steel autoclave for heating at 200 °C for 10 h. The black resultant was respectively washed 3 times with 100 m*l* deionized water and 100 m*l* ethanol and collected by external magnets. Finally, the resultant was dried at 50 °C in a vacuum oven.

Preparation of Fe_3O_4/MCC-PEI

Fe_3O_4/MCC-PEI was prepared by the impregnation method [22]. Briefly, 0.500 g Fe_3O_4/MCC was added into 100 m*l* deionized water which contained a certain amount (2.500 g, 5.000 g, 10.000 g) of PEI with different molecular weights. Then, the suspension was dispersed by ultrasonication for 30 min. Thereafter, the suspension was immersed in an orbital shaker at 50 °C for 24 h with a speed of 150 rpm. After impregnation, the resultant was rinsed 3 times with 100 m*l* of deionized water and 100 m*l* of ethanol and dried overnight at 50 °C. The products obtained from different molecular weights (1.8K, 10K, 70K) and concentrations (2.5 wt%, 5.0 wt%, 10.0 wt%) of PEI were abbreviated as Fe_3O_4/MCC-PEI(1.8K-5), Fe_3O_4/MCC-PEI(10K-5), Fe_3O_4/MCC-PEI(70K-2.5), Fe_3O_4/MCC-PEI(70K-5), Fe_3O_4/MCC-PEI(70K-10), respectively.

Characterization of Materials

A field emission scanning electron microscope (Hitachi SU8020, Japan) and a transmission electron microscope (JEOL 1200EX, Japan) were used to observe the morphology of materials. Elemental analytical instrument (Elementar, vario EL cube, Germany) was used to determine the element content in materials. The crystal phases of materials were analyzed using a powder diffraction-meter (PANalytical, Netherlands) with Cu-Kα radiation (λ=1.544426 Å). FT-IR spectrometer (Nicolet 5700, USA) was used to identify the functional groups with the technology of KBr pellet from 4000-400 cm^{-1}. Thermogravimetric analyzer (STA 2500, Germany) was used to identify the thermal stability of the materials under an air atmosphere. Vibrating sample magnetometer (Quantum Design, USA) was used to measure the magnetic properties of the samples at room temperature. X-ray photoelectron spectroscopy (Escalab 250Xi, ThermoFisher Scientific, USA) was used to determine the chemical environments of C, N, O atoms present on the surface. Zeta potential analyzer (Zetasizer nano ZSP, Malvern, England) was used to measure the zeta potential over the pH range of 2-12.

Adsorption Studies

Batch experiments were performed in 100 m*l* conical flasks at 298 K to evaluate various parameters such as pH, contact time, initial dye concentration, and temperature. The desired solution pH was adjusted by adding a solution of 0.1 M HCl or NaOH. In more detail, 0.020 g Fe_3O_4/MCC-PEI was added into 50 m*l* CR dye solution (pH=7.0±0.2). And then, the mixture was rapidly transferred into a shaker set to a constant speed (150 rpm) and temperature for 24 h. The adsorption isotherm was carried out at three different

temperatures (298±1, 308±1, 318±1 K) and the adsorption kinetics was conducted with different time intervals. After predetermined contact time, the solution pH was measured using a pH meter (Mettler Toledo, FE20). The adsorbent was rapidly separated by a magnet due to the strong magnetic responsiveness of Fe_3O_4/MCC-PEI, and the residual concentration of CR in the supernatant was measured by a TU-1900 UV/Vis spectrophotometer at 500 nm [23]. The equilibrium adsorption capacity (equation (1)) and the removal efficiency (equation (2)) were calculated by the following equations:

$$q_e = \frac{(C_0 - C_e)V}{m} \quad (1)$$

$$R\% = \frac{C_0 - C_e}{C_0} \quad (2)$$

where q_e (mg/g) is the equilibrium adsorption capacity of CR; C_0 and C_e (mg/*l*) are the concentrations of the CR solution initially and at equilibrium, respectively; m (g) is the mass of adsorbent; V (*l*) is the volume of solution; R% is the removal efficiency.

Adsorbent Regeneration

The CR adsorption-desorption cycles onto Fe_3O_4/MCC-PEI(70K-5) were conducted six times. Briefly, 0.020 g Fe_3O_4/MCC-PEI(70K-5) was added into 50 m*l* of CR solution for 24 h and was quickly separated by strong magnets after the adsorption equilibrium was reached. After that, 50 m*l* NaOH solution (1 mol/*l*) was added and shaken for another 2 h. The regenerated adsorbent was washed with 50 m*l* ethanol 3 times and dried at 50 °C in a vacuum oven. The regenerated adsorbent was reused to the next adsorption-desorption cycles and the equilibrium adsorption capacity was calculated by equation (1).

Results and Discussion

Characterizations of the Synthesized Composites

SEM, TEM and Elemental Analysis

SEM and TEM images of MCC, Fe_3O_4/MCC, and Fe_3O_4/MCC-PEI(70K-5) were shown in Figure 1. As observed in Figure 1(a) and (b), the raw microcrystalline cellulose was found to be rod-shaped with a few packed and the surface was wrinkled. Figure 1(c) and (d) showed the micro-morphology of Fe_3O_4/MCC, it was obvious that a large number of Fe_3O_4 nanoparticles adhered to the surface of MCC and the size was uniform. After modification with PEI, the surface of Fe_3O_4/MCC was coated by the polymer. And it can be seen that the nanoparticles were tightly bonded together by polymers (Figure 1(f)). The TEM images of the Fe_3O_4/MCC-PEI(70K-5) were shown in Figure 1(g) and (h), and exhibiting the spherical structure of the Fe_3O_4. The particle size of the Fe_3O_4 can be estimated to be about 70 nm. In addition, the EDS map scanning (Figure 1(i)) confirmed the formation of Fe_3O_4/MCC-PEI(70K-5), which indicated the uniform loading of Fe_3O_4 on the supported MCC and the PEI were homogeneously distributed on the surface of Fe_3O_4/MCC-PEI(70K-5).

Furthermore, the elemental analyzer was used to determine the content of C, H, and N in the adsorbent and the results were shown in Table 1. The amount of C and H greatly decreased after the nano Fe_3O_4 was bonded, which was due to the fact that the Fe_3O_4 does not include C and H elements, and the Fe_3O_4 particles accounted for a large proportion of mass. However, their contents increased after the modification with PEI. Besides, the content of N in Fe_3O_4/MCC-PEI(70K-5) was 1.40 %, which was much higher than that of the others. This indicated that the surface of Fe_3O_4/MCC had been functionalized by PEI.

XRD Analysis

Figure 2 showed the XRD patterns of Fe_3O_4, MCC, Fe_3O_4/MCC, and Fe_3O_4/MCC-PEI(70K-5). The diffraction peaks (2θ) at 30.32 °, 35.69 °, 43.30 °, 53.68 °, 57.16 °, and 62.77 ° in Figure 2(a) could be respectively attributed to the (220), (311), (400), (422), (511), and (440) Miller planes of the cubic-phase Fe_3O_4 with a face-centered cubic structure (JCPDS card no.19-0629) [24]. The peaks at 2θ=14.80 °, 16.20 °, 22.27 °, and 34.51 ° for MCC (Figure 2(b)) were respectively ascribed to $(1\bar{1}0)$, (110), (200), and (004) crystallographic planes (JCPDS no. 00-050-2241) which was consistent with the typical cellulose Iβ diffraction peaks [25]. Compared with pattern (b), the diffraction peaks belonging to MCC were much weaker in patterns (c) and (d) which was due to the magnetization by Fe_3O_4 nanoparticles. Meanwhile, the crystalline form of MCC may be destroyed during the high temperature reaction. In addition, there was a broad but weak diffraction peak can be observed at 2θ= 13.7 °-26.6 ° in pattern (d), suggesting the amorphous PEI had been coated on the surface of Fe_3O_4/MCC [26].

FT-IR Spectroscopy Analysis

The FT-IR spectra of MCC and Fe_3O_4/MCC-PEI(70K-5) were illustrated in Figure 3. As one can see from the spectrum of MCC, the peaks at 3424 and 1622 cm^{-1} could be respectively ascribed to the O-H stretching vibrations and bending vibrations. The peaks at the wavenumber of 2905 cm^{-1} were ascribed to the C-H stretching vibrations. The peaks at 1056 and 1022 cm^{-1} could be assigned to the C-O-C stretching vibrations of the polysaccharide skeletal in MCC, and the peaks at 895 cm^{-1} were attributed to the typical C-H deformation of β-glycosidic in cellulose [27]. Compared with the spectrum of MCC, a sharp and strong adsorption peak can be observed at the wavenumber of 562 cm^{-1}, which was attributed to the Fe-O-Fe stretching vibrations in Fe_3O_4. This suggested that the nano Fe_3O_4 had been successfully synthesized and bonded to the surface of MCC. Besides, the peaks at 1652, 1570, and 1314 cm^{-1} were respectively assigned to the N-H bending vibrations of primary amino,

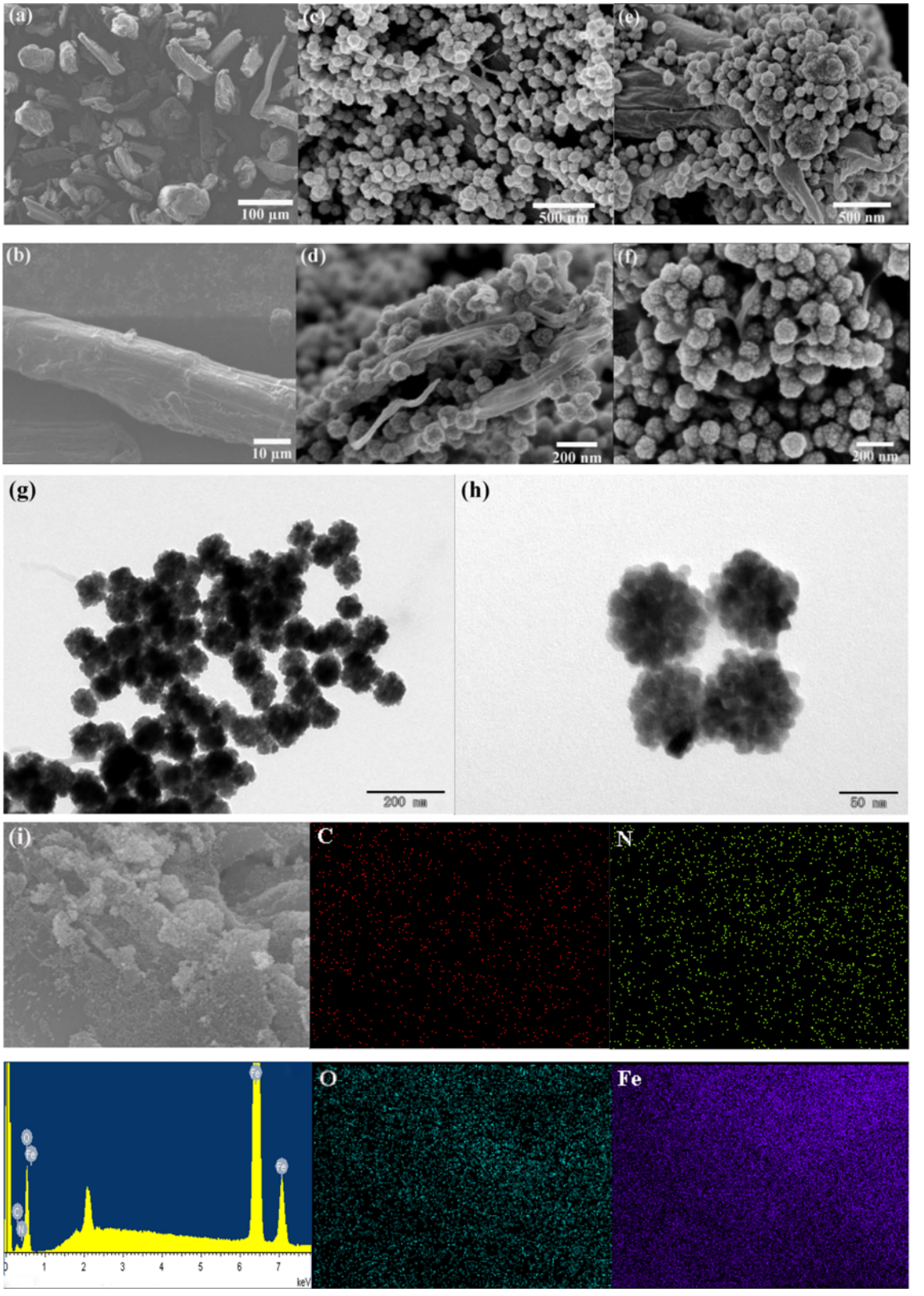

Figure 1. SEM micrographs of MCC (a, b), Fe_3O_4/MCC (c, d), Fe_3O_4/MCC-PEI(70K-5) (e, f), TEM micrographs of Fe_3O_4/MCC-PEI(70K-5) (g, h), EDS mapping of Fe_3O_4/MCC-PEI(70K-5) (i).

Table 1. Data of element analysis of MCC, Fe_3O_4/MCC, and Fe_3O_4/MCC-PEI(70K-5)

Sample	Element content		
	C %	H %	N %
MCC	41.68	6.47	0.16
Fe_3O_4/MCC	19.41	3.02	0.17
Fe_3O_4/MCC-PEI(70K-5)	21.16	3.42	1.40

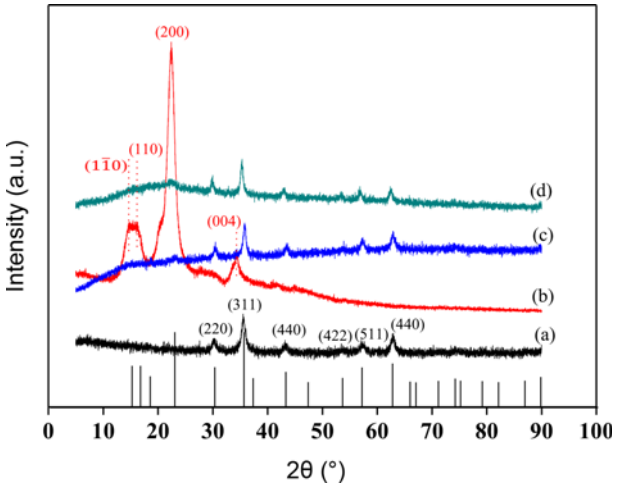

Figure 2. XRD patterns of Fe_3O_4 (a), MCC (b), Fe_3O_4/MCC (c), and Fe_3O_4/MCC-PEI(70K-5) (d).

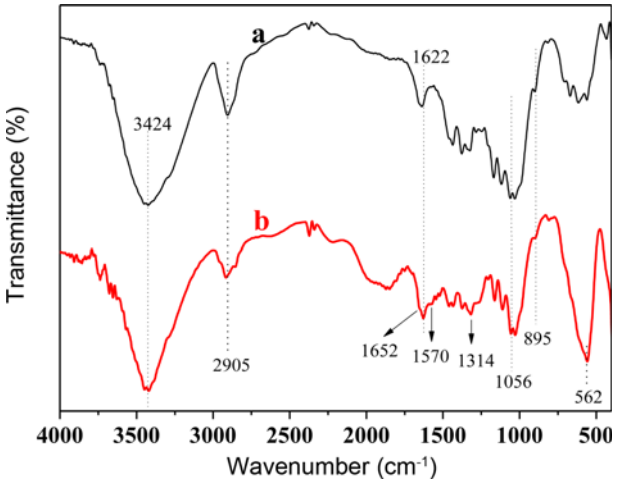

Figure 3. FT-IR spectra of MCC (a) and Fe_3O_4/MCC-PEI(70K-5) (b).

secondary amino, and C-N stretching vibrations [28], which suggested the PEI had been successfully covered on the surface.

TG and DTG Analysis

Thermogravimetric analyses of MCC and Fe_3O_4/MCC-PEI(70K-5) were carried out under air atmosphere from room temperature to 800 °C and the curves of TG and DTG

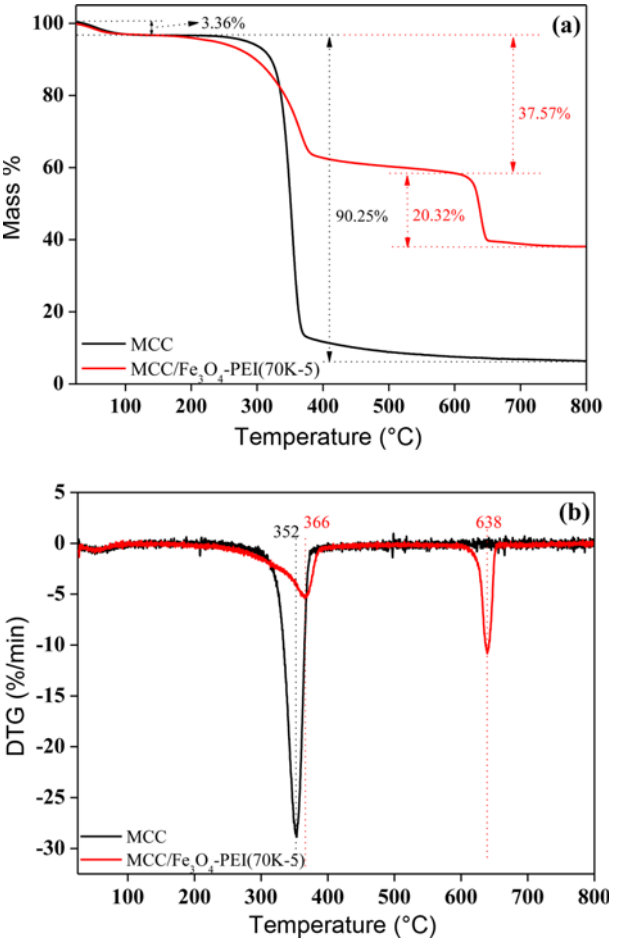

Figure 4. TG (a) and DTG (b) curves of MCC and Fe_3O_4/MCC-PEI(70K-5).

were presented in Figure 4(a) and (b), respectively. As one can see from Figure 4(a), there were two stages for MCC. The first stage occurring before 200 °C with the weight loss of 3.36 % was attributed to the loss of adsorbed moisture. The second stage occurring at 200 °C to 800 °C with the weight loss of 90.25 % was ascribed to the decomposition of MCC. As for Fe_3O_4/MCC-PEI(70K-5), three stages can be observed. The first stage was the same as that of MCC, whereas the second stage was quite different. There was only 37.57 % weight loss for the second stage from the temperature range of 200 °C to 600 °C, which was ascribed to the decomposition of MCC. Furthermore, the third stage occurring at 600 °C to 800 °C with a weight loss of 20.32 % was due to the degradation of PEI. In addition, the peak temperature of DTG corresponding to the thermal decomposition of MCC in Fe_3O_4/MCC-PEI(70K-5) (366 °C) was higher than that of raw MCC (352 °C), which may be due to the PEI or the Fe_3O_4 nanoparticles covered on the surface of MCC, resulting in more difficult thermal decomposition of MCC. This also suggests that the PEI was successfully covered on the Fe_3O_4/MCC surface, and accounted for a

large proportion of the total mass.

Vibrating Sample Magnetometer Analysis

The magnetic properties of Fe_3O_4/MCC, Fe_3O_4/MCC-PEI(70K-5), and CR adsorbed Fe_3O_4/MCC-PEI(70K-5) were measured by vibrating sample magnetometer at room temperature, with a magnetic field from -30000 to 30000 Oe. As one can observe in Figure 5(a), the magnetization saturation values (M_s) of Fe_3O_4/MCC, Fe_3O_4/MCC-PEI(70K-5), and CR adsorbed Fe_3O_4/MCC-PEI(70K-5) were 47.62 emu/g, 43.07 emu/g, and 41.98 emu/g, respectively. It was reasonable that the M_s of Fe_3O_4/MCC-PEI(70K-5) decreased to 43.07 emu/g, which was due to the weakening of PEI coated on the surface. The M_s of CR adsorbed Fe_3O_4/MCC-PEI(70K-5) was the lowest due to the magnetism weakened by the Congo red molecules adsorbed on the surface. The magnetic force, however, was still strong enough to effectively separate CR from the solution. In addition, the coercivity values (H_c) of the materials were 3.47, 2.57, and 1.28 Oe, respectively. The H_c values of all the samples were less than 50 Oe which is the theoretical value for superparamagnetic particles [29]. Hence, the adsorbent showed superparamagnetic characteristics at room temperature. Furthermore, the CR adsorbed Fe_3O_4/MCC-PEI(70K-5) was attracted to the glass wall on the magnet side by the magnet within 10 s (Figure 5(b)). This further proved that the adsorbent can be easily recovered after CR adsorbed.

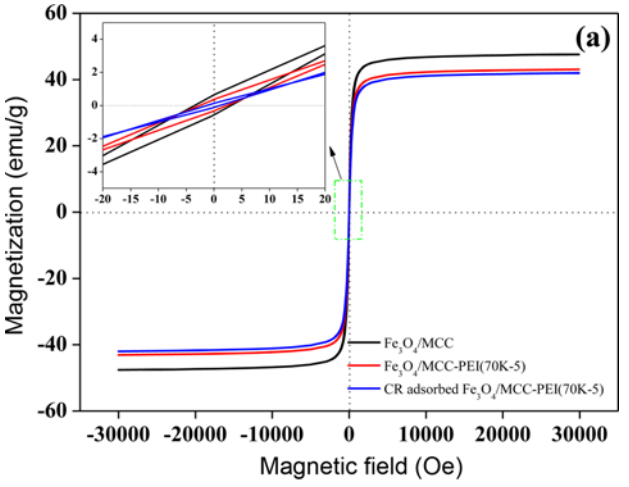

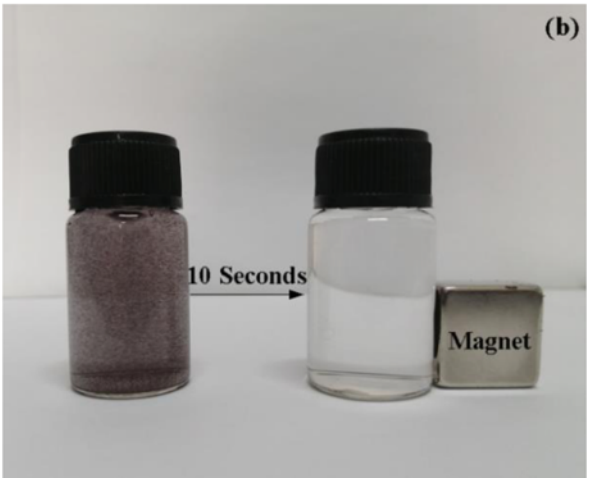

Figure 5. (a) Hysteresis loop of Fe_3O_4/MCC, Fe_3O_4/MCC-PEI(70K-5), and CR adsorbed Fe_3O_4/MCC-PEI(70K-5) and (b) magnetic attraction effect of CR adsorbed Fe_3O_4/MCC-PEI(70K-5).

Textural Properties

The surface area and porosity of porous materials are important characteristics of their applications as adsorbents, which will directly affect the adsorption capacity. The BET surface area and porosity of Fe_3O_4/MCC-PEI(70K-5) were investigated based on N_2 adsorption-desorption isotherms at 77 K (Figure 6). According to the Brunauer-Deming-Deming-Teller classification, the isotherms onto Fe_3O_4/MCC-PEI(70K-5) can be defined as type IV with H3 hysteresis loop, which is characteristic of mesoporous materials [7]. The hysteresis loops of Fe_3O_4/MCC-PEI(70K-5) at a relative pressure range of 0.8-1 indicated the presence of large mesopores and macrospores. The BET surface area (multipoint method: P/P_0=0.070-0.300) of Fe_3O_4/MCC-PEI(70K-5) was 20.363 m^2/g and pore volume was 0.132 cm^3/g. In addition, the Barrett-Joyner-Halenda (BJH) desorption pore diameter distribution of Fe_3O_4/MCC-PEI(70K-5) was shown in the inserted image in Figure 6. Different pore sizes were observed in Fe_3O_4/MCC-PEI(70K-5), and the pore size distribution was in the range of 2.16 to 69.59 nm. The high specific surface area, mesoporous channels, and unique pore distribution of Fe_3O_4/MCC-PEI(70K-5) could benefit the contact between the adsorption sites and adsorbates [2], and then enhance the adsorption capacity.

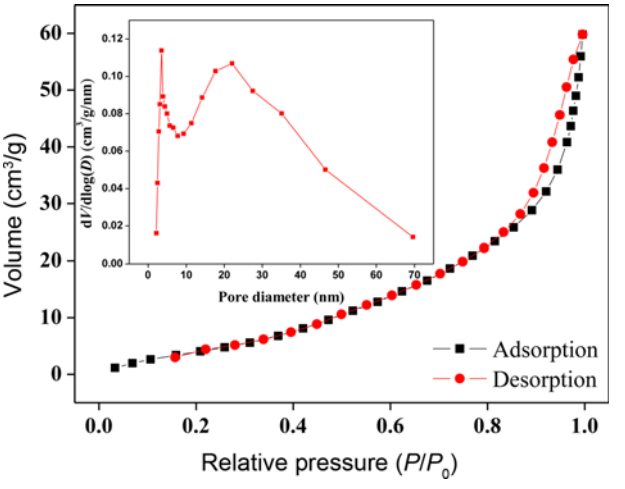

Figure 6. (a) Nitrogen adsorption/desorption isotherms of Fe_3O_4/MCC-PEI(70K-5). The inserted image was the pore size distribution.

Determination of the Optimal PEI Covered on Fe_3O_4/MCC

The molecular weight and the amount of PEI coated on the surface were important for CR adsorption onto Fe_3O_4/MCC-PEI. A higher molecular weight of PEI can improve the adsorption performance, while too much PEI coated may reduce the adsorption capacity [30]. So the optimal PEI coated should be investigated. Herein, a series of Fe_3O_4/MCC-PEI composites was fabricated through altering the amount of the PEI coated while maintaining the constant Fe_3O_4/MCC amount (0.500 g) and the adsorption experiments were investigated at 298 K. The effects of the molecular weight and the amount of PEI on adsorption capacities were respectively shown in Figure 7(a) and (b). As one can see from Figure 7(a), the adsorption capacity of Fe_3O_4/MCC-PEI(70K-5) was significantly stronger than that of Fe_3O_4/MCC-PEI(1.8K-5) and Fe_3O_4/MCC-PEI(10K-5). This was because the higher molecular weight of PEI can adsorb more protons, which means higher adsorption performance. In addition, as seen in Figure 7(b), the adsorption capacities of Fe_3O_4/MCC-PEI(70K-10) and Fe_3O_4/MCC-PEI(70K-5) were significantly stronger than that of Fe_3O_4/MCC-PEI(70K-2.5), and Fe_3O_4/MCC exhibited the weakest adsorption capacity. Hence, the amount of PEI covered on Fe_3O_4/MCC has a direct effect on CR adsorption. This was mainly because the PEI covered on the Fe_3O_4/MCC surface carries a large amount of primary amine group ($-NH_2$), which can be protonated and positively charged in aqueous solution. Since CR is a kind of anionic dye with the sulfonate groups, the CR adsorption will be enhanced due to the electrostatic attraction. Nevertheless, the amount of PEI coated on the Fe_3O_4/MCC surface was limited. Once the amount of PEI coated on the surface reached saturation, it did not change even after the PEI concentration in solution was increased. In this work, the adsorption performance and mechanisms onto Fe_3O_4/MCC-PEI(70K-5) were studied.

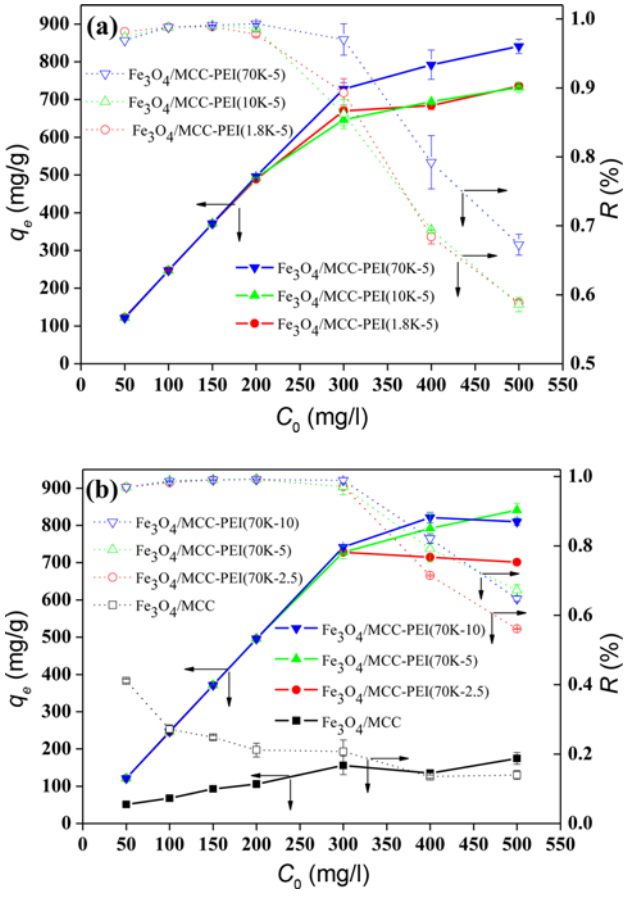

Figure 7. Removal efficiency and adsorption capacity of Fe_3O_4/MCC and Fe_3O_4/MCC-PEI at different initial concentrations (T: 298 K, pH 7.0, t: 24 h).

Adsorption Kinetics

The effect of contact time on adsorption capacity of Fe_3O_4/MCC-PEI(70K-5) for CR was investigated with various initial concentrations at a constant temperature (298±1 K). As shown in Figure 8(a), the rate of CR adsorption was very fast at the beginning of the experiments during the first 20 min, and about 80 % of the maximum adsorption amount was reached. And then, the adsorption amount of CR increased gradually with the prolonged contacted time until the adsorption equilibrium was achieved. This can be explained by the fact that the active sites on Fe_3O_4/MCC-PEI(70K-5) surfaces were completely exposed in aqueous solution at the beginning, and the CR molecules in solution rapidly occupied the adsorption sites. Afterwards, a slow and stable growth process was followed. This was mainly due to the CR molecules that had been adsorbed on the surface will repel the residual free molecules to be adsorbed. Thus, the remaining empty active sites will be more difficult to occupy by the residual CR molecules in the solution.

In order to further study the mechanisms of CR adsorption onto Fe_3O_4/MCC-PEI(70K-5), pseudo-first-order (equation (3)), pseudo-second-order (equation (4)), and intra-particle diffusion model (equation (5)) were used to examine the kinetic data. The three models [31] are generally expressed as follows:

$$q_t = q_e(1-e^{-K_1 t}) \tag{3}$$

$$q_t = \frac{K_2 q_e^{\,2} t}{1+K_2 q_e t} \tag{4}$$

$$q_t = K_{id} t^{1/2} + C \tag{5}$$

where q_e and q_t (mg·g^{-1}) are the adsorption capacities at equilibrium and at time t (min), respectively; K_1 (min^{-1}), K_2 (g·(mg·min)$^{-1}$), and K_{id} (mg·(g·min$^{1/2}$)$^{-1}$) are the equilibrium rate constants of pseudo-first-order, pseudo-second-order,

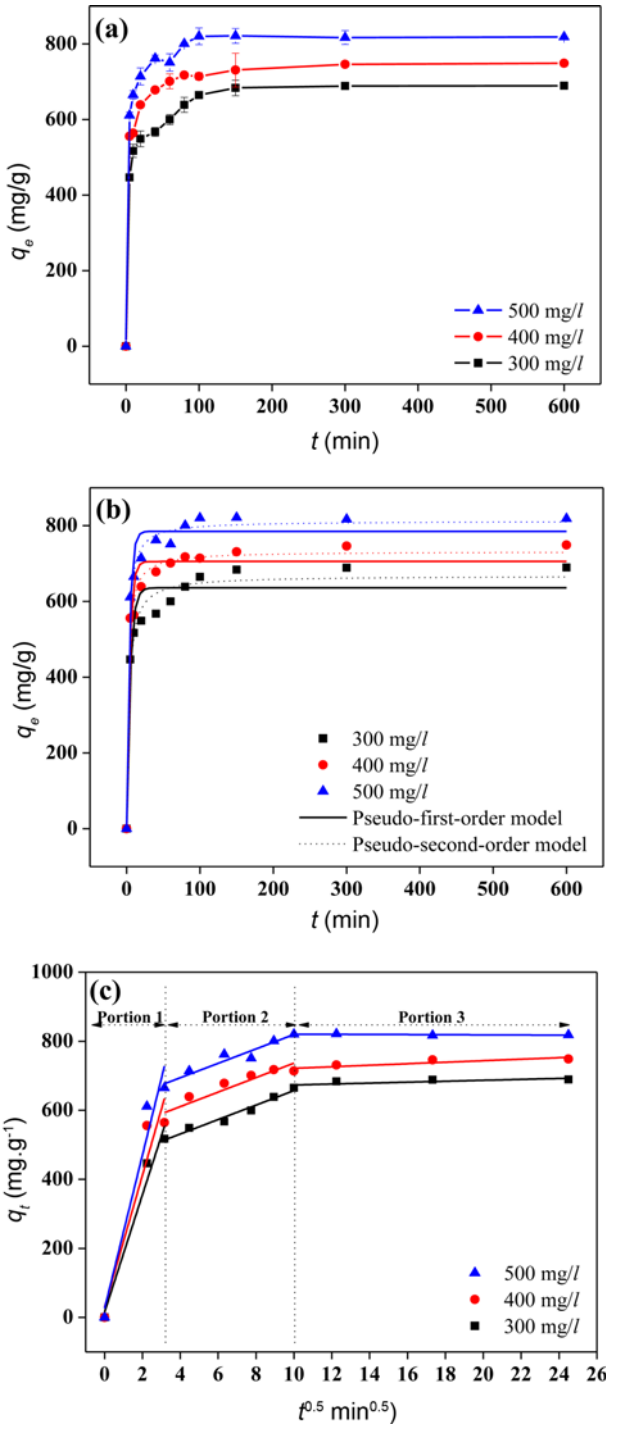

Figure 8. Adsorption capacity vs. time in different concentrations (a), adsorption kinetics of CR fitted with pseudo-first-order kinetic and pseudo-second-order kinetic (b) and intra-particle diffusion model (c) (T: 298 K, pH 7.0).

and intra-particle diffusion model, respectively. C (mg·g^{-1}) is a constant describing the thickness of boundary layer.

Figure 8(b) and (c) showed the fitting results of CR adsorption onto Fe_3O_4/MCC-PEI(70K-5) using the pseudo-first-order model, pseudo-second-order model, and intra-particle diffusion model, and the fitting parameters were outlined in Table 2. According to R^2 values (representing the goodness of fit), the values calculated from pseudo-second-order model (> 0.97) were all higher than that of pseudo-first-order model (>0.93), which indicated the pseudo-second-order model can better fit for the experimental data and describe the adsorption process. Furthermore, the values of $q_{e,cal}$ calculated from pseudo-second-order models were more close to the experimental adsorption amount $q_{e,exp}$, which further indicated that the CR adsorption onto Fe_3O_4/MCC-PEI(70K-5) obeys the pseudo-second-order kinetic model for the whole adsorption period, and chemical adsorption was predominant during the adsorption process.

Since the above kinetic model could not determine the diffusion mechanism, the intra-particle diffusion model proposed by Weber and Morris was used to further understand the adsorption behavior of CR on Fe_3O_4/MCC-PEI(70K-5) [32]. Figure 8(c) exhibited the fitting results of the intra-particle diffusion model on Fe_3O_4/MCC-PEI(70K-5). The adsorption process consisted of three portions for the different initial concentrations. The first steep linear portion was external diffusion, which represents the binding of CR molecules through active sites distributed on the outer surface of the adsorbent. The second linear portion is intra-particle diffusion, which represents the binding of CR molecules through adsorption sites distributed on the inner surface. The last linear portion was suggested to be the final equilibrium, which indicates the establishment of equilibrium [17]. Initially, the CR molecule was adsorbed by the adsorption sites on the outer surface of Fe_3O_4/MCC-PEI(70K-5), which was a rapid adsorption process. When the outer surface was saturated and no empty adsorption sites could be occupied, the CR molecules began to enter the pores of the adsorbent and were adsorbed by the adsorption sites on the inner surface [33]. Furthermore, it was found that the linear line of the intra-particle diffusion did not pass through the origin ($C \neq 0$ in Table 2), indicating the intra-particle diffusion was not the sole rate-controlling step and the external diffusion may also be significant in rate-controlling step due to the large values of C [34]. Therefore, the adsorption mechanism was regarded as predominantly chemisorption and the adsorption process was controlled by the external diffusion and intra-particle diffusion.

Adsorption Isotherms and Thermodynamics

Adsorption Isotherms

Adsorption isotherms were carried out at three different temperatures to explore the adsorption mechanism onto Fe_3O_4/MCC-PEI(70K-5). Langmuir model and Freundlich model are widely used to describe the equilibrium adsorption isotherms. Langmuir model (equation (6)) commonly describes monolayer adsorption, which assumes the adsorbent surface

Table 2. Kinetic model parameters and constants with statistical data

C_0	$q_{e,exp}$	Pseudo-first-order model			Pseudo-second-order model		
		$q_{e,cal}$	K_1	R^2	$q_{e,cal}$	K_2	R^2
300	689.11	636.05	0.2031	0.9341	667.85	0.0005	0.9759
400	748.65	705.34	0.2491	0.9553	732.00	0.0006	0.9880
500	818.39	785.03	0.2612	0.9679	812.44	0.0006	0.9918
C_0	$q_{e,exp}$	Intra-particle diffusion model					
		Portion-1			Portion-2		
		C	$K_{id,1}$	R^2	C	$K_{id,2}$	R^2
300	689.11	14.91	170.1804	0.9477	447.63	20.9341	0.9670
400	748.65	29.00	191.3561	0.8513	526.81	20.9825	0.8440
500	818.39	26.08	221.9845	0.9079	610.84	20.8630	0.9172

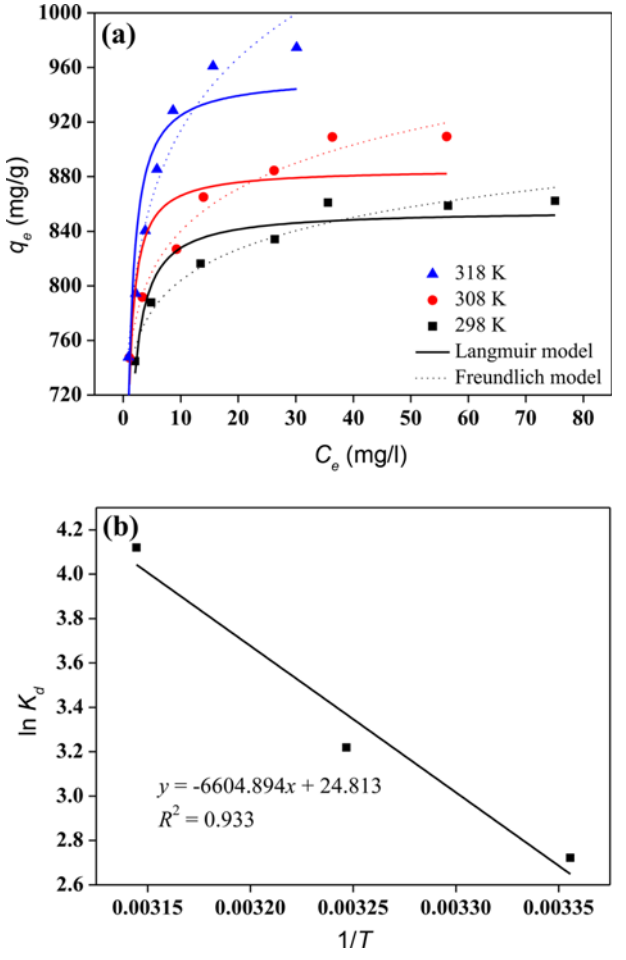

Figure 9. Adsorption isotherms of CR on Fe_3O_4/MCC-PEI(70K-5) (a) and plot of lnK_d versus 1/T for CR adsorption (b) (pH 7.0, t: 24 h).

is uniform and the adsorption energy is equal everywhere. Furthermore, one active site can only be occupied by one molecule and there is no interaction between adsorbed molecules [35]. While Freundlich model (equation (7)) is an empirical equation applicable to adsorption on a heterogeneous surface as well as multilayer adsorption. The nonlinear form equations of the above adsorption models [36] are as follows:

Table 3. Isotherm parameters for adsorption of CR on Fe_3O_4/MCC-PEI(70K-5)

T (K)	Langmuir			Freundlich		
	q_{max}	K_L	R^2	K_F	n	R^2
298	855.51	2.979	0.894	732.624	24.783	0.951
308	885.79	4.381	0.745	744.794	19.113	0.978
318	954.15	3.156	0.820	757.992	12.306	0.952

$$q_e = \frac{K_L q_{\max} C_e}{1 + K_L C_e} \tag{6}$$

$$q_e = K_F C_e^{1/n} \tag{7}$$

where q_e (mg·g^{-1}) is the amount of CR adsorbed at equilibrium; C_e (mg·l^{-1}) is the equilibrium concentration of CR; K_L is the Langmuir binding constant which is related to the energy of adsorption; $q_{\max}$ (mg·g^{-1}) is the maximum adsorption capacity of CR; K_F and n are Freundlich constants related to adsorption capacity and adsorption intensity, respectively. All of the constants were calculated by fitting the equations.

The application of Langmuir and Freundlich models to the CR adsorption on Fe_3O_4/MCC-PEI(70K-5) were exhibited in Figure 9(a), and the fitting results were listed in Table 3. As shown in Figure 9(a), a higher temperature favored the adsorption capacities. In addition, the R^2 values obtained at different temperatures were all > 0.95 for the Freundlich model, which were significantly larger than that of Langmuir model. The results showed that Freundlich model can well fit the adsorption isotherm and adsorption process of CR on Fe_3O_4/MCC-PEI(70K-5), and it followed the multi-site adsorption mechanism on the heterogeneous surface. In

addition, the K_F values represent the strength of the interaction between adsorbent and adsorbates, and the higher K_F values indicate the higher affinity. As shown in Table 3, the strongest interaction occurred at 318 K, and the weakest interaction occurred at 298 K, which is consistent with the experimental data of adsorption capacity.

Thermodynamics

In order to evaluate the adsorption behavior, the adsorption of CR onto Fe_3O_4/MCC-PEI(70K-5) was investigated at three different temperature (298, 308, 318 K). The values of thermodynamic parameters such as the Gibbs free energy (ΔG^o), enthalpy (ΔH^o), and entropy (ΔS^o) were obtained from experiments using the following equations:

$$K_d = \frac{C_0 - C_e}{C_e}\frac{V}{m} \tag{8}$$

$$\ln K_d = \frac{\Delta S^0}{R} - \frac{\Delta H^0}{RT} \tag{9}$$

$$\Delta G^0 = -RT \ln K_d \tag{10}$$

where K_d is the thermodynamic distribution coefficient of adsorbent; C_0 and C_e (mg·l^{-1}) are initial concentration and equilibrium concentration, respectively; V (l) is the volume of CR solution and m (g) is the mass of Fe_3O_4/MCC-PEI(70K-5); R is the universal gas constant (8.314 J·(mol·K)$^{-1}$) and T (K) is the reaction temperature. A straight line was obtained by plotting K_d versus $1/T$, the ΔH^o values and ΔS^o values were calculated according to the slope and intercept of the straight line (Figure 9(b)).

Thermodynamic parameters obtained from the CR adsorption onto Fe_3O_4/MCC-PEI(70K-5) were listed in Table 4. As exhibited, the value of ΔS^o (206.295 J·mol^{-1}·K^{-1}) was positive in the temperature range of 298 to 318 K, indicating the increase of disorder. It may be related to the structure change of adsorbate or adsorbent [37]. Besides, the value of ΔH^o (54.913 kJ·mol^{-1}) was positive, which indicated that the adsorption process on the surface of the adsorbent is an endothermic process, and the higher temperature is beneficial to the increase of the adsorption capacity. Additionally, the ΔG^o values were all negative, indicating the adsorption process is spontaneous under different environment temperatures. Meanwhile, it was also found that the values of ΔG^o decreased with the increase of temperature, further indicating that the adsorption of CR by Fe_3O_4/MCC-PEI(70K-5) was more favorable at higher temperatures.

Table 4. Thermodynamic parameters for CR adsorption

T (K)	ln(K_d)	ΔG^o (kJ·mol^{-1})	ΔH^o (kJ·mol^{-1})	ΔS^o (J(mol·K)$^{-1}$)
298	2.7214	-6.7424		
308	3.2188	-8.2423	54.9131	206.2953
318	4.1202	-10.8932		

CR concentration: 400 mg/*l*.

Effect of Ionic Strength

The cations Na^+, K^+, Ca^{2+}, and Mg^{2+} existing in natural water may interact with the adsorbent and adsorbate, and then the surface chemistry will be affected. Therefore, it is of great significance to study the influence of cations on CR adsorption. Figure 10 showed the effect of cations on adsorption, and the adsorption capacities were enhanced by the addition of extra cations. The adsorption amount of Fe_3O_4/MCC-PEI(70K-5) increased steadily with the increase of Na^+ and K^+ concentration in solution. Electrostatic interactions are considered to be a very important factor in the adsorption process. Previous researches have reported that electrostatic interactions will be affected when additional cations are added. This is due to the fact that some salt ions will reach the surface and then change the surface conditions of the adsorbent. The Na^+, K^+ covered on the surface of adsorbent would also become active sites to form complexes with CR molecules during the CR adsorption process, which favors the CR adsorption onto adsorbent [38]. In addition, the cations may neutralize the repulsion between the free CR molecules and the CR molecules adsorbed on Fe_3O_4/MCC-PEI(70K-5) in solution, which also leads to an increase in CR adsorption. Compared with Na^+ and K^+, it was found that at the same concentration, the enhancement of Ca^{2+} and Mg^{2+} was stronger. This is because Ca^{2+} and Mg^{2+} have a higher positive charge than that of Na^+ and K^+ [39]. Additionally, this may be also owing to the salting-out effect produced by Ca^{2+} and Mg^{2+} which would make the solubility of CR reduced [40]. The precipitated CR molecules are

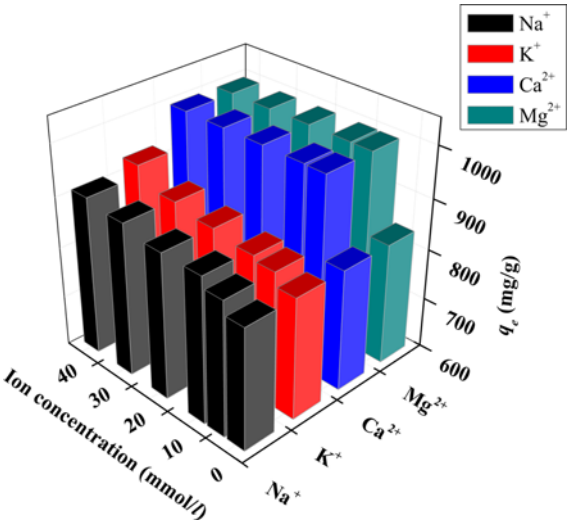

Figure 10. Effect of ionic strength on CR adsorption (CR concentration: 400 mg/*l*, T: 298 K, pH 7.0, t: 24 h).

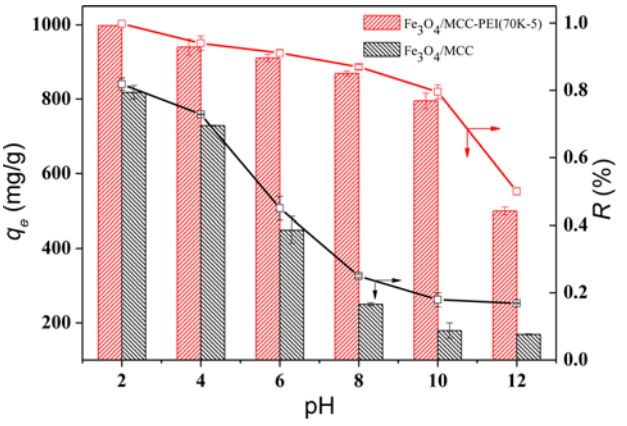

Figure 11. Effect of solution pH on CR adsorption (CR concentration: 400 mg/*l*, T: 298 K, t: 24 h).

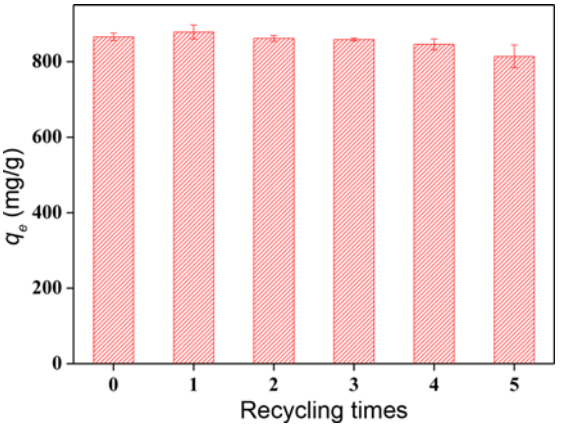

Figure 12. Recycling performance on CR adsorption (CR concentration: 400 mg/*l*, T: 298 K, pH 7.0, t: 24 h).

more easily adsorbed onto the surface of Fe_3O_4/MCC-PEI(70K-5).

Effect of pH

The pH value of the solution is one of the important factors affecting the adsorption capacity, which affects the surface charge and binding sites of the adsorbent and the ionization of the adsorbate molecules. The impact of pH on the removal of CR from aqueous solution was tested in the range of 2-12. As shown in Figure 11, the adsorption capacity of CR decreased with the pH increasing and the adsorption amount of Fe_3O_4/MCC-PEI(70K-5) was much higher than that of Fe_3O_4/MCC. The adsorption amount reached 997.69 mg/g at pH value of 2 (the color turned to be dark blue at pH value of 2 and 4), while it was only 499.43 mg/g at pH value of 12 (the color was red in the pH range of 6-12). This may be due to the different properties of adsorbents and adsorbates in various pH environments. The Congo red molecules existing in dissociated form as anionic dye ions with negatively charged (dye-SO_3^-) in solution. Under strongly acidic conditions, the amino groups carried by Fe_3O_4/MCC-PEI(70K-5) will be protonated to form positively charged sites such as -NH_3^+, resulting in an electrostatic attraction to the negatively charged CR molecules, leading to an increase in removal efficiency. However, the protonation of amino groups will be weakened with the increase of solution pH, resulting in the weakening of electrostatic interactions. Furthermore, the existence of excess -OH^- ions in solution may compete with the CR molecules for the decreasing number of positively charged sites on the surface of Fe_3O_4/MCC-PEI(70K-5) as the pH increased. This makes the adsorption process become more difficult. Thereby, the adsorption capacity of the adsorbent at high pH was significantly lower than that at low pH.

Regeneration and Reuse Tests

The regeneration of CR adsorbed Fe_3O_4/MCC-PEI(70K-5) is very important for the application of Fe_3O_4/MCC-PEI(70K-5), especially in commercial applications. In this study, Fe_3O_4/MCC-PEI(70K-5) was subjected to six consecutive adsorption-desorption experiments to test the regeneration performance. In previous reports, various reagents such as methanol, ethanol, chloroform, acetone, HCl solution, and NaOH solution were used as eluent [41], and the NaOH solution was found to be the most effective, ethanol was second to it. Figure 12 showed the efficiency of CR adsorption onto Fe_3O_4/MCC-PEI(70K-5) with the treatment of the NaOH solution (1 mol/*l*) and washing by ethanol. It was found that the adsorption amount exhibited a downward trend with the adsorption times increasing, but the reduction for each time was not large. The adsorption amount was 814.15 mg/g after recycling 5 times, accounting for 94.04 % of the original adsorption amount, which was still a very high efficiency. The results showed that the obtained Fe_3O_4/MCC-PEI(70K-5) has good recyclability and can be easily regenerated. While a small loss of the adsorption efficiency may be attributed to the fact that treatment with NaOH and ethanol cannot completely remove the CR molecules adsorbed at the previous adsorption step, and it was also considered to be the washing loss at each time of the adsorbent.

Possible Adsorption Mechanism

The zeta potentials of Fe_3O_4/MCC and Fe_3O_4/MCC-PEI(70K-5) at different pH values were shown in Figure 13(a). As exhibited, the values of zeta potential decreased gradually with pH increasing and the zeta potentials of Fe_3O_4/MCC-PEI(70K-5) were all higher than that of Fe_3O_4/MCC. The overall trend was consistent with the influence of pH on adsorption capacity. The points of zero charge (pH_{zpc}) of them were estimated to be about 6.78 and 10.93 mV, respectively. Therefore, the surfaces of composites were positively charged at pH < pH_{zpc}, which was favorable for the binding of negatively charged CR molecules. In addition,

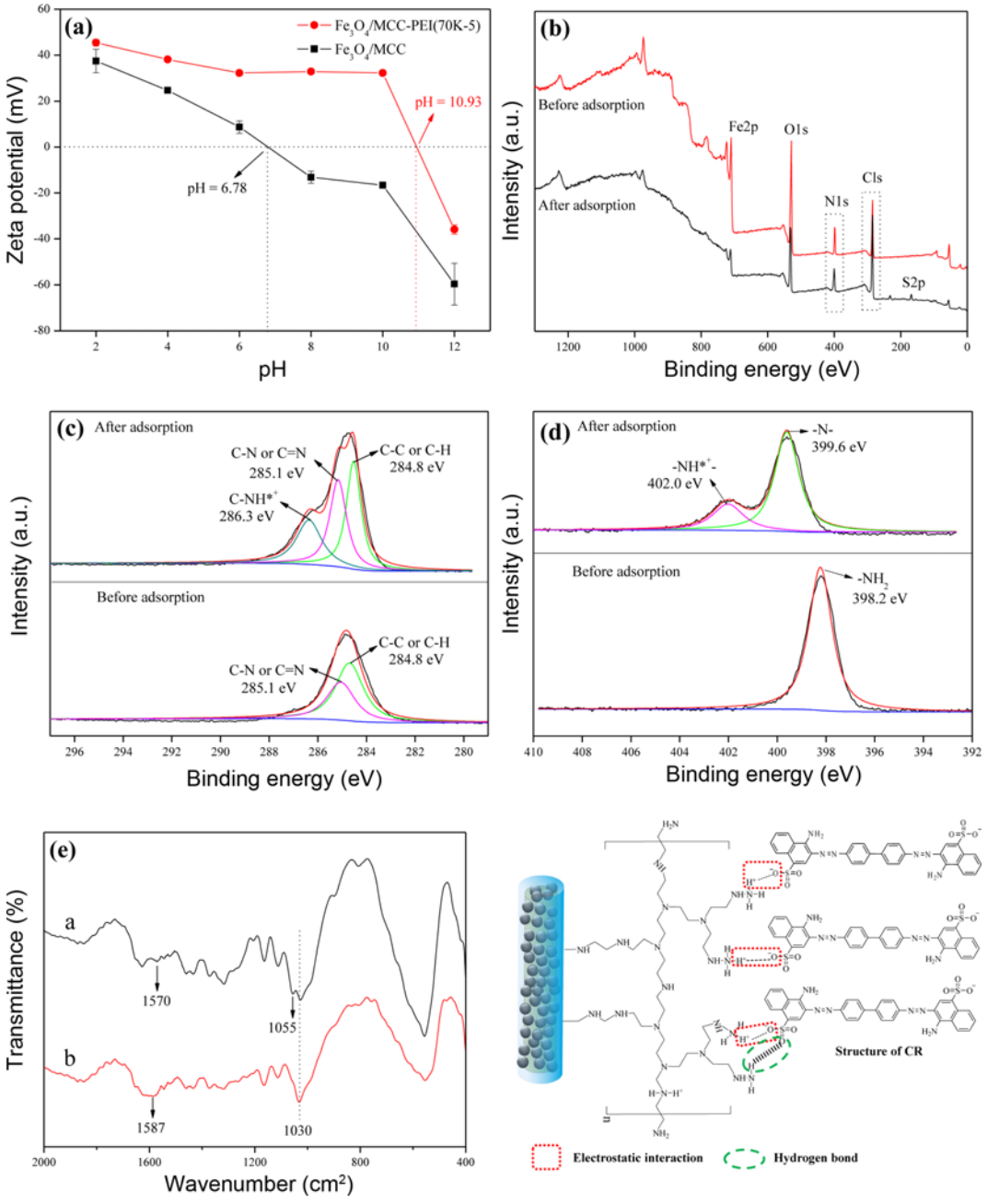

Figure 13. (a) Effect of solution pH on the zeta potential of Fe_3O_4/MCC and Fe_3O_4/MCC-PEI(70K-5), (b) XPS spectra of Fe_3O_4/MCC-PEI(70K-5) before and after adsorption, (c) C1s spectrum, (d) N1s spectrum, (e) FT-IR spectra of Fe_3O_4/MCC-PEI(70K-5) before and after adsorption, and (f) possible mechanism for CR adsorption onto Fe_3O_4/MCC-PEI(70K-5).

the zeta potentials of Fe_3O_4/MCC-PEI(70K-5) higher than that of Fe_3O_4/MCC can be attributed to the fact that the PEI coated on the surface contains a large number of amines, which are prone to be protonated and positively charged in solution. Meanwhile, the CR molecules will be doubly negatively charged because of the dissociation of Na^+. Therefore, the electrostatic interactions between adsorbent and adsorbate with opposite charges will be enhanced. While at pH > 10.93, the surface of Fe_3O_4/MCC-PEI(70K-5) will be negatively charged, which will greatly weaken the electrostatic interactions between the adsorbents and adsorbates, thus hindering the adsorption process.

To further understand the interaction mechanism between Fe_3O_4/MCC-PEI(70K-5) and CR molecules, the XPS spectra of the samples before and after adsorption were recorded, as plotted in Figure 13(b)-(d). A wide-scan spectrum of Fe_3O_4/

MCC-PEI(70K-5) before and after adsorption can be observed in Figure 13(b). The peak of Fe2p was derived from the Fe_3O_4 nanoparticles, which suggested the successful magnetization of the adsorbent. The appearance of N1s peaks on XPS spectrum of Fe_3O_4/MCC-PEI(70K-5) proved the existence of PEI. And the new peak of S2p can be observed in the spectrum after adsorption, indicating the adsorbed CR molecules on the surface. Furthermore, the C1s and N1s spectra of adsorbent before and after adsorption were compared (Figure 13(c) and (d)). Figure 13(c) showed the C1s spectra of Fe_3O_4/MCC-PEI(70K-5) before and after adsorption. The photoelectron peaks at 284.8 and 285.1 eV were ascribed to the binding energy of C-C or C-H and C-N or C=N and a new photoelectron peak appeared at the position of 286.3 eV, which was ascribed to the binding energy of C-NH*$^+$. This was due to the fact that the amino groups were prone to be protonated and the CR molecules were adsorbed by the electrostatic interaction. In addition, the chemical environment of N had changed a lot. As exhibited in Figure 13(d), there was a strong photoelectron peak located at 398.2 eV, which was attributed to the binding energy -NH_2. However, the -NH_2 photoelectron peak disappeared after adsorption, and two new photoelectron peaks at 399.6 and 402.0 eV were observed, which was corresponding to binding energies of -N- and -NH*$^+$-, respectively [42]. The -NH*$^+$- came from the binding of amino groups with CR molecules via electrostatic interactions.

Furthermore, Figure 13(e) showed the FT-IR spectra of the adsorbent before and after adsorption. As exhibited in the spectra, one can see that the adsorption peak at 1030 cm^{-1} was much broader than before adsorption and the intensity of adsorption peak at 1055 cm^{-1} decreased. This was due to the adsorption peak at 1059 cm^{-1} of S=O was overlapped [7]. In addition, a broad adsorption peak was observed at 1587 cm^{-1}, which was ascribed to N=N stretching vibrations, in the spectrum after adsorption [43]. These indicated that the CR molecules had been adsorbed onto the surface of the adsorbent. Additionally, a significant change was found at the adsorption band of 1570 cm^{-1}, assigned to secondary amino. It became much weaker after CR adsorption. This could be ascribed to the ionic salt formation between the amino groups and CR molecules, which greatly reduced the vibration frequency of N-H bonds [39]. The formation model was mainly electrostatic interactions between the adsorbents and adsorbates. Besides, the hydrogen bonding between the amino groups of PEI and O of -SO_3^- on the surface of CR molecules may also act [44].

The above analysis showed that the protonation of amino groups played an important role in the whole adsorption process, and the CR molecules were tightly adsorbed on the adsorbent surface by complexing with -NH*$^+$- via electrostatic interactions. In addition, the hydrogen bonding between the PEI and CR molecules also enhanced the adsorption process. The possible mechanism for CR adsorption onto Fe_3O_4/MCC-PEI(70K-5) was illustrated in Figure 13(f).

Conclusion

Fe_3O_4/MCC-PEI(70K-5) was synthesized with a simple method and characterized by SEM, TEM, XRD, FT-IR, TGA, and BET techniques. The removal efficiencies of CR by Fe_3O_4/MCC-PEI with different amounts and molecular weights of PEI coated were compared, and the adsorption capacity of Fe_3O_4/MCC-PEI(70K-5) was studied. The kinetics data suggested that the adsorption process of CR onto Fe_3O_4/MCC-PEI(70K-5) fitted well with pseudo-second-order kinetic model. The equilibrium adsorption capacity of Fe_3O_4/MCC-PEI(70K-5) was measured and fitted with Langmuir and Freundlich models. It was found that the experimental data was the most suitable for the Freundlich model. And the adsorption process followed a multi-site adsorption mechanism on a heterogeneous surface. It was known from the thermodynamic data that the adsorption process on the surface of Fe_3O_4/MCC-PEI(70K-5) was endothermic. Besides, Fe_3O_4/MCC-PEI(70K-5) has excellent adsorption efficiency in low pH environment and the adsorption capacities were greatly affected by additional cations, especially Ca^{2+} and Mg^{2+} ions. Regeneration studies demonstrated that Fe_3O_4/MCC-PEI(70K-5) could be regenerated with high reusability for the efficient removal of CR. Additionally, the possible adsorption mechanism based on strong electrostatic interactions is critical throughout the adsorption process.

Acknowledgements

This work was financially supported by National Natural Science Foundation of China (Grant No. 51568048, No. 21276121).

References

1. L. Hu, Z. Yang, L. Cui, Y. Li, H. H. Ngo, Y. Wang, Q. Wei, H. Ma, L. Yan, and B. Du, *Chem. Eng. J.*, **287**, 545 (2016).
2. L. You, C. Huang, F. Lu, A. Wang, X. Liu, and Q. Zhang, *Int. J. Biol. Macromol.*, **107**, 1620 (2018).
3. V. S. Munagapati and D. Kim, *Ecotox. Environ. Safe.*, **141**, 226 (2017).
4. U. Habiba, T. A. Siddique, T. C. Joo, A. Salleh, B. C. Ang, and A. M. Afifi, *Carbohydr. Polym.*, **157**, 1568 (2017).
5. H. Jalife-Jacobo, R. Feria-Reyes, O. Serrano-Torres, S. Gutiérrez-Granados, and J. M. Peralta-Hernández, *J. Hazard. Mater.*, **319**, 78 (2016).
6. C. Ma, F. Wang, C. Zhang, Z. Yu, J. Wei, Z. Yang, Y. Li, Z. Li, M. Zhu, L. Shen, and G. Zeng, *Chemosphere*, **168**, 80 (2017).
7. C. Lei, M. Pi, C. Jiang, B. Cheng, and J. Yu, *J. Colloid Interface Sci.*, **490**, 242 (2017).

8. M. O. Ansari, R. Kumar, S. A. Ansari, S. P. Ansari, M. A. Barakat, A. Alshahrie, and M. H. Cho, *J. Colloid Interface Sci.*, **496**, 407 (2017).
9. Q. Wang, A. Tang, L. Zhong, X. Wen, P. Yan, and J. Wang, *Powder Technol*., **339**, 872 (2018).
10. S. Madan, R. Shaw, S. Tiwari, and S. K. Tiwari, *Appl. Surf. Sci.*, **487**, 907 (2019).
11. L. Han, F. Ge, G. Sun, X. Gao, and H. Zheng, *Dalton Trans.*, **48**, 4650 (2019).
12. V. S. Munagapati, V. Yarramuthi, Y. Kim, K. M. Lee, and D. Kim, *Ecotoxicol. Environ. Saf.*, **148**, 601 (2018).
13. R. Fan, H. Min, X. Hong, Q. Yi, W. Liu, Q. Zhang, and Z. Luo, *J. Hazard. Mater.*, **364**, 780 (2019).
14. T. A. Saleh, M. M. Al-Shalalfeh, and A. A. Al-Saadi, *Sens. Actuators B*, **254**, 1110 (2018).
15. N. You, X. Wang, J. Li, H. Fan, H. Shen, and Q. Zhang, *J. Ind. Eng. Chem.*, **70**, 346 (2019).
16. A. Shamsizadeh, M. Ghaedi, A. Ansari, S. Azizian, and M. K. Purkait, *J. Mol. Liq.*, **195**, 212 (2014).
17. T. Ai, X. Jiang, Q. Liu, L. Lv, and H. Wu, *Bioresour. Technol.*, **273**, 8 (2019).
18. F. Rafieian, M. Mousavi, Q. Yu, and M. Jonoobi, *Int. J. Biol. Macromol.*, **130**, 280 (2019).
19. K. Gerulová, A. Bartošová, L. Blinová, K. Bártová, M. Dománková, Z. Garaiová, and M. Palcut, *Algal Res.*, **33**, 165 (2018).
20. X. Li, Z. Wang, J. Ning, M. Gao, W. Jiang, Z. Zhou, and G. Li, *J. Environ. Manage.*, **217**, 305 (2018).
21. C. Jiang, X. Wang, D. Qin, W. Da, B. Hou, C. Hao, and J. Wu, *J. Hazard. Mater.*, **369**, 50 (2019).
22. S. Wong, H. H. Tumari, N. Ngadi, N. B. Mohamed, O. Hassan, R. Mat, and N. A. Saidina Amin, *J. Cleaner Prod.*, **206**, 394 (2019).
23. H. N. Tran, S. You, A. Hosseini-Bandegharaei, and H. Chao, *Water Res.*, **120**, 88 (2017).
24. M. S. Moorthy, D. Seo, H. Song, S. S. Park, and C. Ha, *J. Mater. Chem. A*, **1**, 12485 (2013).
25. A. D. French, *Cellulose*, **21**, 885 (2014).
26. J. Geng, Y. Yin, Q. Liang, Z. Zhu, and H. Luo, *Chem. Eng. J.*, **361**, 1497 (2019).
27. X. Yu, S. Tong, M. Ge, J. Zuo, C. Cao, and W. Song, *J. Mater. Chem. A*, **1**, 959 (2013).
28. S. Deng, G. Zhang, S. Chen, Y. Xue, Z. Du, and P. Wang, *J. Mater. Chem. A*, **4**, 15851 (2016).
29. A. Morel, S. I. Nikitenko, K. Gionnet, A. Wattiaux, J. Lai-Kee-Him, C. Labrugere, B. Chevalier, G. Deleris, C. Petibois, A. Brisson, and M. Simonoff, *ACS Nano*, **2**, 847 (2008).
30. D. Shu, F. Feng, H. Han, and Z. Ma, *Chem. Eng. J.*, **324**, 1 (2017).
31. L. Zhang, T. Xu, X. Liu, Y. Zhang, and H. Jin, *J. Hazard. Mater.*, **197**, 389 (2011).
32. Y. Zhang, F. Jin, Z. Shen, R. Lynch, and A. Al-Tabbaa, *J. Hazard. Mater*., **347**, 461 (2018).
33. D. Kumar and J. P. Gaur, *Bioresour. Technol.*, **102**, 633 (2011).
34. R. Fan, H. Min, X. Hong, Q. Yi, W. Liu, Q. Zhang, and Z. Luo, *J. Hazard. Mater.*, **364**, 780 (2019).
35. S. Li, M. He, Z. Li, D. Li, and Z. Pan, *J. Mol. Liq.*, **230**, 520 (2017).
36. S. Xu, X. Jiang, L. Liu, Z. Wang, X. Zhang, Y. Peng, and M. Cao, *Environ. Sci. Pollut. Res.*, **26**, 24062 (2019).
37. C. Liu, R. Jin, X. Ouyang, and Y. Wang, *Appl. Surf. Sci.*, **408**, 77 (2017).
38. J. Wang, C. Zheng, S. Ding, H. Ma, and Y. Ji, *Desalination*, **273**, 285 (2011).
39. K. Lu, T. Wang, L. Zhai, W. Wu, S. Dong, S. Gao, and L. Mao, *J. Colloid Interface Sci.*, **539**, 553 (2019).
40. C. Dong, W. Chen, C. Liu, Y. Liu, and H. Liu, *Colloids Surf., A*, **446**, 179 (2014).
41. J. K. Sahoo, S. K. Paikra, M. Mishra, and H. Sahoo, *J. Mol. Liq.*, **282**, 428 (2019).
42. T. Wen, Q. Fan, X. Tan, Y. Chen, C. Chen, A. Xu, and X. Wang, *Polym. Chem.*, **7**, 785 (2016).
43. Z. Zhang, L. Moghaddam, I. M. O. Hara, and W. O. S. Doherty, *Chem. Eng. J.*, **178**, 122 (2011).
44. X. Quan, Z. Sun, H. Meng, Y. Han, J. Wu, J. Xu, Y. Xu, and X. Zhang, *J. Solid State Chem.*, **270**, 231 (2019).